RGD-Modified Apoferritin Nanoparticles for Efficient Drug Delivery to Tumors

Zipeng Zhen,[†,‡] Wei Tang,[†,‡] Hongmin Chen,[†,‡] Xin Lin,[§] Trever Todd,[†,‡] Geoffrey Wang,[†,‡] Taku Cowger,[†,‡] Xiaoyuan Chen,[§] and Jin Xie[†,‡,*]

[†]Department of Chemistry, University of Georgia, Athens, Georgia 30602, United States, [‡]Bio-Imaging Research Center (BIRC), University of Georgia, Athens, Georgia 30602, United States, and [§]National Institute of Biomedical Imaging and Bioengineering (NIBIB), National Institutes of Health (NIH), 31 Center Drive, Bethesda, Maryland 20852, United States

ABSTRACT Ferritin (FRT) is a major iron storage protein found in humans and most living organisms. Each ferritin is composed of 24 subunits, which self-assemble to form a cage-like nanostructure. FRT nanocages can be genetically modified to present a peptide sequence on the surface. Recently, we demonstrated that Cys-Asp-Cys-Arg-Gly-Asp-Cys-Phe-Cys (RGD4C)-modified ferritin can efficiently home to tumors through RGD—integrin $\alpha_v\beta_3$ interaction. Though promising, studies on evaluating surface modified ferritin nanocages as drug delivery vehicles have seldom been reported. Herein, we showed that after being precomplexed with Cu(II), doxorubicin can be loaded onto RGD modified apoferritin nanocages with high efficiency (up to 73.49 wt %). When studied on U87MG subcutaneous tumor models, these doxorubicin-loaded ferritin nanocages showed a longer circulation half-life, higher tumor uptake, better tumor growth inhibition, and less cardiotoxicity than free doxorubicin. Such a technology might be extended to load a broad range of therapeutics and holds great potential in clinical translation.

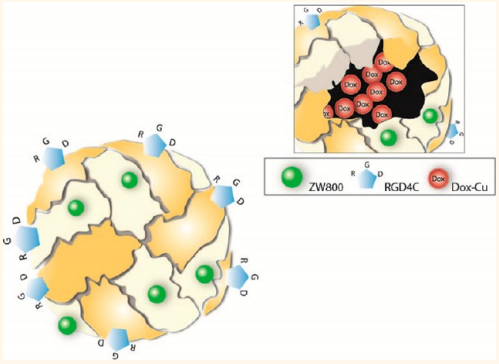

KEYWORDS: ferritin · drug delivery · integrin $\alpha_v\beta_3$ · nanocarrier · doxorubicin

Ferritin (FRT) is a major iron storage protein found in humans and many living organisms. Each FRT nanocage is composed of 24 subunits, which self-assemble to form a cage-like nanostructure, with external and internal diameters of 12 and 8 nm, respectively.[1] In nature, the interiors of FRTs are filled with iron. When expressed artificially in iron-free conditions, the yielded apoferritins are hollow, comprising a cavity that can be loaded with different species. We previously demonstrated that Cu radioisotopes can be encapsulated into FRT nanocages, possibly by association with the metal binding sites at the FRT interiors.[2] Others have reported on using FRTs as nanoreactors to grow metallic nanoparticles.[3−5] Moreover, it was found that metal-containing compounds, such as Gd-DO3A,[6] cisplatin,[7] and desferrioxamine B,[8] can be encapsulated into FRTs. Loading non-metal-containing molecules into FRTs, on the other hand, has seldom been reported.

Our recent investigations showed that nonmetal-containing drug molecules can be precomplexed with a transition metal like Cu(II) and subsequently internalized into FRT interiors. In particular, we found that doxorubicin (Dox), a wide-spectrum anticancer antibiotic, can be efficiently loaded onto FRT nanocages through this method. We report herein the first *in vivo* study on utilizing surface modified FRT nanocages as a drug carrier for Dox-based chemotherapy (Figure 1a).

There are several reasons that we are interested in using surface modified FRTs as a drug delivery system. (1) Biosafety: FRT is a major iron storage protein in humans and therefore is biocompatible and nonimmunogenic. (2) Size: Compared with many other drug carriers, FRTs are much smaller in size. This may lead to a longer circulation half-life and a better tumor accumulation rate. (3) Unique nanostructure: Despite the rigidness under physiological conditions, the FRT nanocages can be broken down into subunits in an acidic environment (*e.g.*, pH = 2).[1] Interestingly, such a process is reversible. When the pH is tuned back to neutral, the FRT subunits

* Address correspondence to jinxie@uga.edu.

Received for review December 16, 2012 and accepted May 29, 2013.

Published online May 29, 2013
10.1021/nn305791q

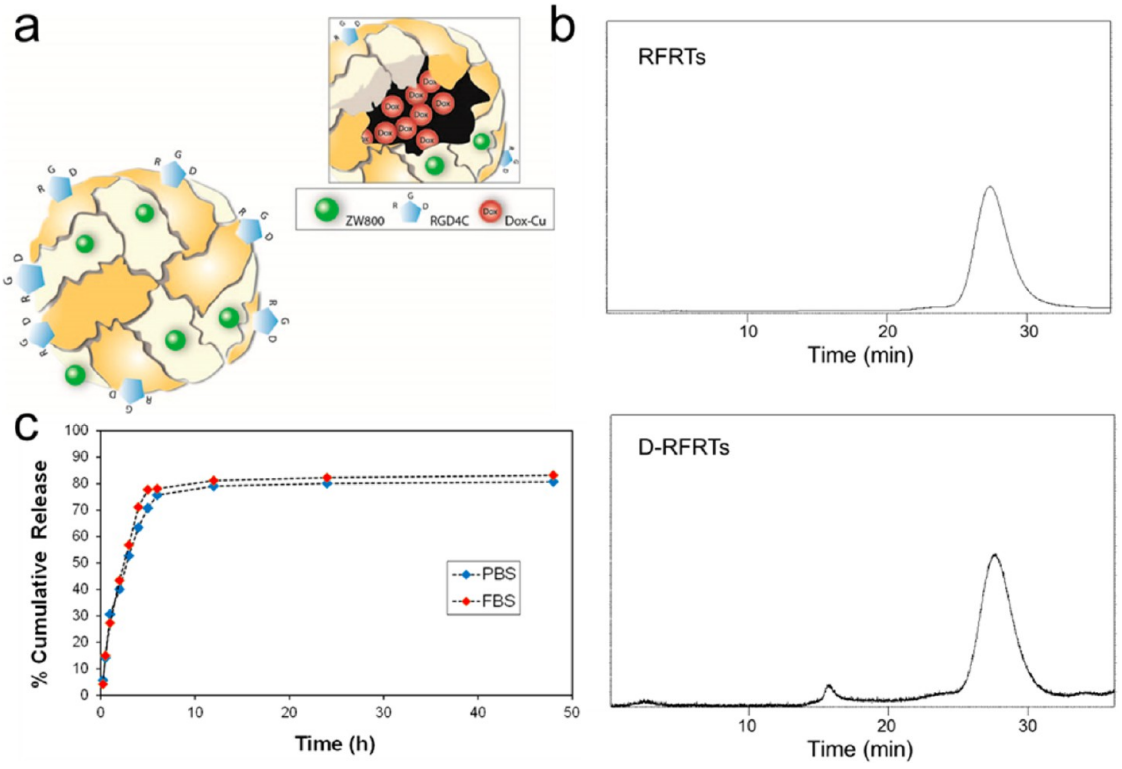

Figure 1. (a) Schematic illustration of D-RFRTs. Dox was precomplexed with Cu, and then encapsulated into RFRTs. (b) Gel-filtration chromatography analysis of RFRTs and D-RFRTs. The same peak at around 27.4 min was observed for both RFRTs and D-RFRTs. (c) Cumulative drug release curves of D-RFRTs in PBS (pH 7.4) and FBS.

will be reconstituted into a nanocage structure, and almost in an intact fashion.[2] As shown in our previous studies, such a pH dependent disassembly and reassembly can be employed to construct hybrid FRT nanocages[9] and to achieve functionality loading into the cavity.[2] (4) The surface of FRTs can be easily modified, either genetically or chemically. We previously conjugated dye molecules,[2] quencher molecules,[9] and peptides[9] onto FRT surface by forming covalent bonds with surface lysine. Genetic modification of FRT has also been reported. In particular, Uchida *et al.* introduced Cys-Asp-Cys-Arg-Gly-Asp-Cys-Phe-Cys (RGD4C), an RGD derivative, onto the FRT surface.[10] RGD is a three-amino-acid sequence with high affinity toward integrin $\alpha_v\beta_3$, a tumor angiogenesis biomarker that is up-regulated on tumor endothelial cells and many types of tumor cells.[11−14] Our previous positron emission tomography (PET) and near-infrared fluorescence (NIRF) imaging studies showed that these RGD4C modified FRTs (RFRTs) can efficiently home to tumors through RGD−integrin interaction and the enhanced permeability and retention (EPR) effect.[2] These features and observations inspired the current investigation of looking into the potential of RFRTs as a drug carrier.

RESULTS AND DISCUSSION

We used human heavy-chain FRTs/RFRTs throughout the study. The expression, production, and purification of FRTs/RFRTs were reported previously.[2] Sodium dodecyl sulfate−polyacrylamide gel electrophoresis (SDS-PAGE) studies found bands at ~22 and ~28 kDa for FRT and RFRT products (Figure S1), correlating well with the molecular weights of their subunits. The yields were 2.5 mg/100 mL cell culture for FRTs and 0.5 mg/100 mL for RFRTs, respectively. Dynamic light scattering (DLS) found a larger size for RFRTs (18.7 nm, Figure S2) than that for FRTs (8.2 nm). This size increase has been attributed to the imparted RGD4C sequence on the FRT surface.

Free Dox shows a relatively low loading rate with either FRTs or RFRTs (Table 1, Supporting Information). To facilitate the loading, we investigated using Cu(II), Mn(II), Zn(II) and Fe(III), all of which are known to be able to form a complex with Dox,[15,16] as a helper agent. Briefly, we incubated Dox−metal complexes with FRT/RFRT nanoparticles. Unloaded drug was removed by passing through a NAP-5 column. The use of Mn(II) and Zn(II) led to a very low FRT/RFRT yield (Table 1, Supporting Information). When Cu(II) or Fe(III) were used, on the other hand, we observed a significantly improved Dox loading, with Cu(II) being the more efficient one (Table 1, Supporting Information). For RFRTs, precomplexation with Cu increased Dox loading rate to 73.49 wt %, in comparison to that of 14.14 wt % for free Dox. Disassembling RFRT nanocages was found to be associated with a low production yield and the approach was not used. It is noted that preincubating RFRTs with Cu(II) can significantly block the drug

loading (down to 8.28 wt %; Table 1, Supporting Information). Our previous studies with ^{64}Cu showed that free copper was mainly loaded into the cavity of RFRTs, possibly by association with the interior metal binding sites. The fact that free Cu(II) can block the Dox−Cu loading indicates that the complex competes for the same binding sites at the interiors of nanocages. Therefore, it is deduced that for empty RFRTs, the drug is mostly encapsulated into the nanocages rather than loaded on the surface.

A gel-filtration chromatography study was performed to evaluate the size change over the drug loading. For RFRTs, we found a single peak at 27.37 min (Figure 1b). This peak was shown on the spectrum of Dox-loaded RFRTs (D-RFRTs) at the same position (27.40 min), indicating that for the majority of the product, the size remained unchanged. This supports the hypothesis that Dox−Cu was encapsulated into the interiors of RFRTs, otherwise a decrease in retention time would have been observed. Notably, a small peak at 15.53 min was found on the spectrum of D-RFRTs. This is attributed to a small portion of particle clustering that was formed during the drug loading, which, according to chromatogram integration, accounts for only 3.53% of the overall product. This result correlates well with the atomic force microscopy (AFM) observation, which found a slightly increased degree of particle clustering after drug loading, albeit an overall comparable size (18.32 ± 4.09 nm for RFRTs and 19.72 ± 2.28 nm for D-RFRTs; Figure S3). Dynamic light scattering (DLS) analysis showed that the size of D-RFRTs was 21.03 nm, which is comparable to that of RFRTs (Figure S2). D-RFRTs were very stable in PBS and showed no precipitation for weeks when kept at a concentration lower than 0.5 mg/mL.

The release of Dox from D-RFRTs was studied in PBS at 37 °C. Unlike Cu(II) that remains bound to the interiors of nanocages,[2] Dox was found to be gradually released from the nanocarriers (Figure 1c). We also studied drug release in fetal bovine serum (FBS). It is well-known that Cu-based complexes are susceptible to transchelation in the serum for its association with serum proteins.[2,17] If Dox−Cu was immobilized onto the surface of RFRTs, incubation in the serum would result in a dramatically accelerated drug release compared to PBS. The results, however, showed an overall comparable release rate (Figure 1c).

We next studied the selectivity of D-RFRTs against integrin $\alpha_v\beta_3$ (Figure 2a). We incubated D-RFRTs with U87MG cells, a human glioblastoma cell line which overexpresses integrin $\alpha_v\beta_3$ on the surface.[18−20] To facilitate the tracking, we labeled the RFRTs with ZW800, a near-infrared dye molecule (ex/em: 780/800 nm).[21] D-RFRTs efficiently bound with U87MG cells and internalized (Figure 2a). Co-incubation with free c(RGDyK) (20×) significantly inhibited the uptake (Figure S4), indicating that the targeting was mainly mediated by RGD-integrin interaction. While at early time points, both RFRTs (ZW800) and Dox were distributed in the cytoplasm, Dox was found predominantly in the nuclei at late time points (Figure S5). This is because Dox was gradually released from the nanocarriers and diffused into the nuclei, where it intercalated with DNA to induce cell death.[22] MTT assays were performed with D-RFRTs against U87MG cells, which found a concentration-dependent cytotoxicity (Figure 2b). It is worth mentioning that no significant toxicity was observed with Cu(II)-loaded RFRTs (Figure 2b). This is not surprising because the toxicity of Cu(II) usually occurs when it is in a free form.[23] As observed in our previous studies, Cu(II) remained bound to RFRT interiors[2] and hence, would not cause extra cytotoxicity.

We intravenously (iv) injected D-RFRTs and free Dox (5 mg Dox/kg) into normal mice, and studied the circulation half-lives of D-RFRTs and free Dox by analyzing the Dox contents in the blood at different time points (Figure 2c). Free Dox showed a quick washout from the circulation and a short half-life of 6.5 min, which is similar to our previous observations.[22] For D-RFRTs, we observed a biphasic plasma concentration profile with a second phase $t_{1/2}$ of 27 h (Figure 2c, simulation performed with software WinNonlin). As mentioned above, Cu-based complexes are easily subjected to transchelation in the blood.[17] Such a significantly extended half-life again supports the hypothesis that Dox was mostly located at the interiors of the nanocages.

We then used NIRF imaging to study the tumor selectivity of D-RFRTs in a subcutaneous U87MG tumor model. ZW800-labeled D-RFRTs (5 mg Dox/kg) were iv injected and images were taken at selected time points on a Maestro II system. Results from 24 h are shown in Figure 3a. Strong activities from ZW800 were observed in the tumor areas with a tumor-to-normal-tissue ratio of 55. Immediately after the imaging at 24 h, the animals were sacrificed. The tumors as well as major organs were harvested, placed on a sheet of black paper, and subjected to an *ex vivo* imaging study (Figure 3a). We found that the activities in the tumor were two times higher than those in the liver, and the accumulation in other organs was low (Figure 3b).

We also studied the distribution of Dox (ex/em: 480/570 nm). Unlike the observation with ZW800, we found a low tumor-to-normal-tissue contrast from *in vivo* imaging (0.11, Figure 3a). This was attributed to the strong tissue autofluorescence from the animal skin as the excitation/emission of Dox lies in the visible spectrum window. Indeed, *ex vivo* Dox imaging exhibited a biodistribution pattern that was similar to the ZW800 results (Figure 3a). As a comparison, free Dox at the same dose was injected in a control group. In that case, both *in vivo* and *ex vivo* imaging found a much lower tumor uptake (Figure 3a,b).

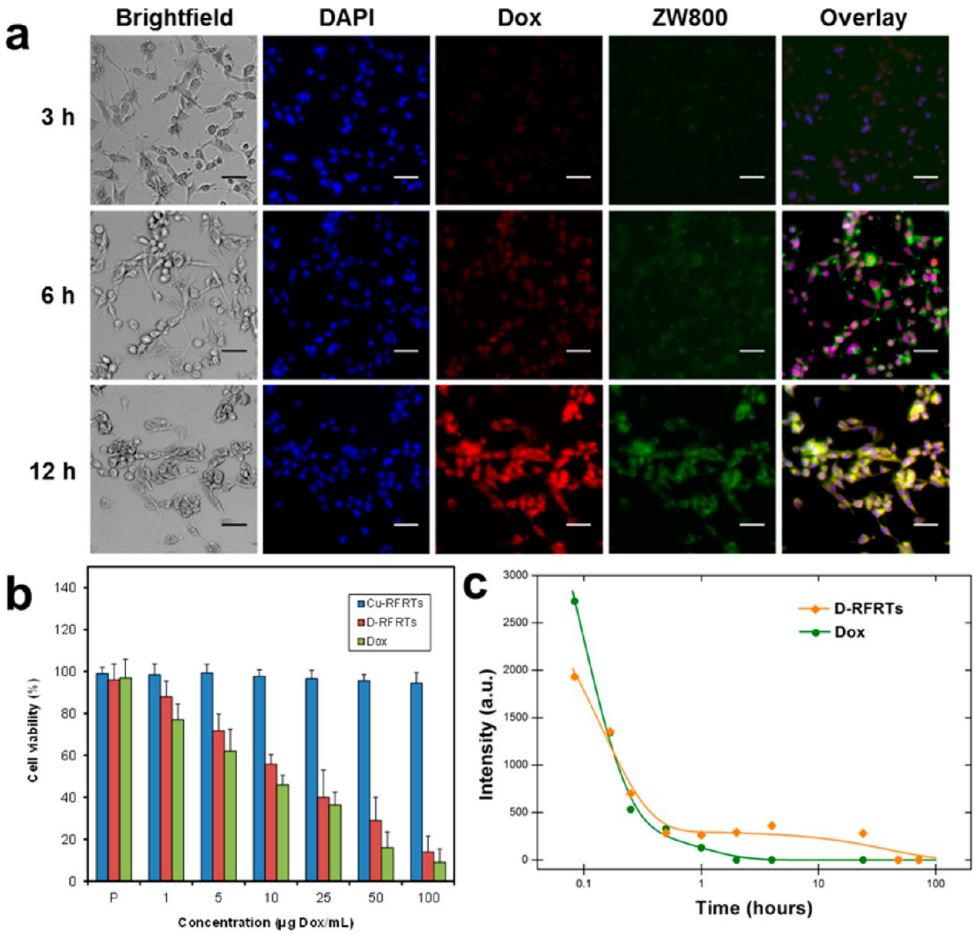

Figure 2. (a) Time dependent uptake of ZW800-labeled D-RFRTs by U87MG cells. Blue, DAPI; red, Dox; green, ZW800. Scale bar, 50 μm. (b) Viability assay results of U87MG cells with D-RFRTs, free Dox, and Cu-bearing RFRTs. (c) Plasma Dox concentrations at different time points after iv injection of D-RFRTs or free Dox into healthy nude mice.

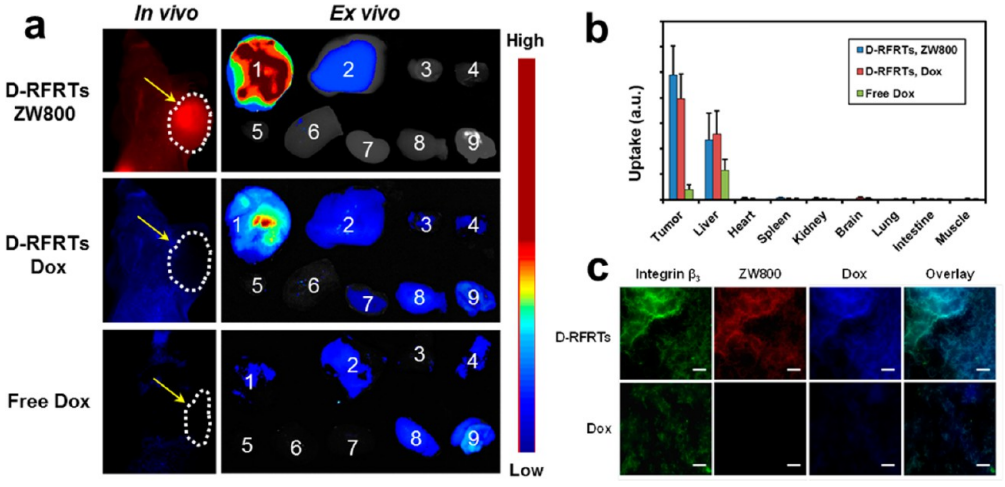

Figure 3. (a) *In vivo* and *ex vivo* imaging results of U87MG tumor-bearing mice injected with ZW800-labeled D-RFRTs and free Dox. For *ex vivo* studies, the organs were arranged in the following order: 1, tumor; 2, liver; 3, lung; 4, muscle; 5, heart; 6, spleen; 7, kidneys; 8, brain; 9, intestine. (b) Column histograms of fluorescence activities in different organs obtained from the *ex vivo* imaging data. (c) Immunohistology results from tumor sections. Good overlap was found between RFRTs (ZW800) and positive integrin β_3 staining, indicating that the targeting was mainly mediated by RGD-integrin interaction. Dox, on the other hand, displayed a diffusive distribution pattern, suggesting the release of Dox from the carriers. Green, Cy5.5; red, ZW800; blue, Dox. Scale bar, 50 μm.

Histology studies were performed with the tumor tissues (Figure 3c). Good correlation was observed between RFRT (ZW800) and anti-integrin β_3 staining (Cy5), suggesting that the targeting was mainly

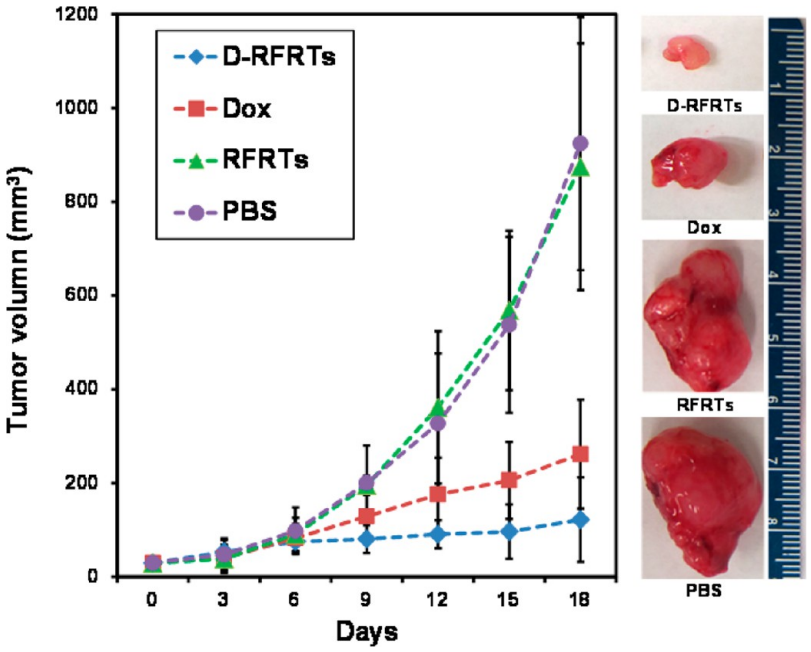

Figure 4. (a) Therapy studies performed on U87MG tumor-bearing nude mice (n = 5/group). On day 18, significant difference in tumor growth was found between D-RFRT treated mice and those treated with PBS, RFRTs and free Dox ($P < 0.05$). Eighteen days after the onset of the treatment, a TGI rate of 89.6% was observed for D-RFRTs, in comparison to that of 74.0% for free Dox.

mediated by RGD-integrin interaction. Notably, most of the nanocarriers remained within the blood vessels, likely caused by association with integrins expressed on endothelial cells. On the other hand, Dox showed a more disseminated distribution pattern as many of the activities were found outside of the vessels. It indicates that Dox was released from the nanocages and diffused into the interstitial space and tumor cells.

A therapeutic study was performed in U87MG subcutaneous tumor models. Briefly, D-RFRTs (5 mg Dox/kg) were iv injected every three days for two weeks (n = 5). In the control groups, PBS, RFRTs, and free Dox at the same dose were injected (n = 5). Eighteen days after the start of the treatment, D-RFRT group showed a tumor volume of 122.02 ± 80.35 mm^3, compared to that of 924.34 ± 269.57 mm^3 for the PBS group and 874.97 ± 253.6 mm^3 for the RFRT group (Figure 4). This represents a tumor growth inhibition (TGI) rate of 89.6%, which is significantly higher than that of 74.0% for free Dox ($p < 0.05$). No significant weight loss was observed with the D-RFRT treated mice (Figure S6).

Cardiotoxicity has been one major limiting factor in Dox-based therapy.[24] To study this, we performed caspase-3 staining on the heart tissues from both Dox and D-RFRT treated mice (Figure 5a). A much lower level of positive staining was observed with the D-RFRT group, indicating mitigated toxicity by using RFRTs as a drug carrier. Similarly, H&E staining found necrosis in the tumors treated with D-RFRT, but no obvious pathological abnormalities such as hemorrhage, edema, lymphocyte infiltration and necrosis in major organs including the heart (Figure 5b and Figure S7).

CONCLUSIONS

We showed that precomplexation with Cu(II) can significantly improve the loading of Dox onto RFRT nanocages. Such a metal-assisted Dox loading has been observed previously with liposome-based nanocarriers,[25,26] though with a different mechanism. Gel-filtration chromatography found an overall unchanged nanoparticle size, suggesting that the drug was mostly internalized into the cavity of the particles. This was supported by the observations made in the drug release and circulation half-life studies, which found no sign of copper transchelation when exposing D-RFRTs to serum proteins. Also, it was found that the loading of Dox−Cu can be efficiently blocked by free Cu(II), which is known to be encapsulated into the interiors of RFRTs. There are both threefold and fourfold symmetric channels present on FRT surface.[27] The threefold channel is hydrophilic and usually serves as a pathway to transfer metal cations in and out of the protein cage, with a potential gradient directing toward the cavity of the nanocages.[27] The fourfold channel, on the other hand, has a potential gradient in the opposite direction, and is believed to be used to expel species from the cavity.[27] The fact that the internalization of Dox−Cu can be blocked by free Cu(II) suggests that the complex is taken up through a similar mechanism as free metal cations do. It is postulated that complexation with Cu(II) provides a driving force

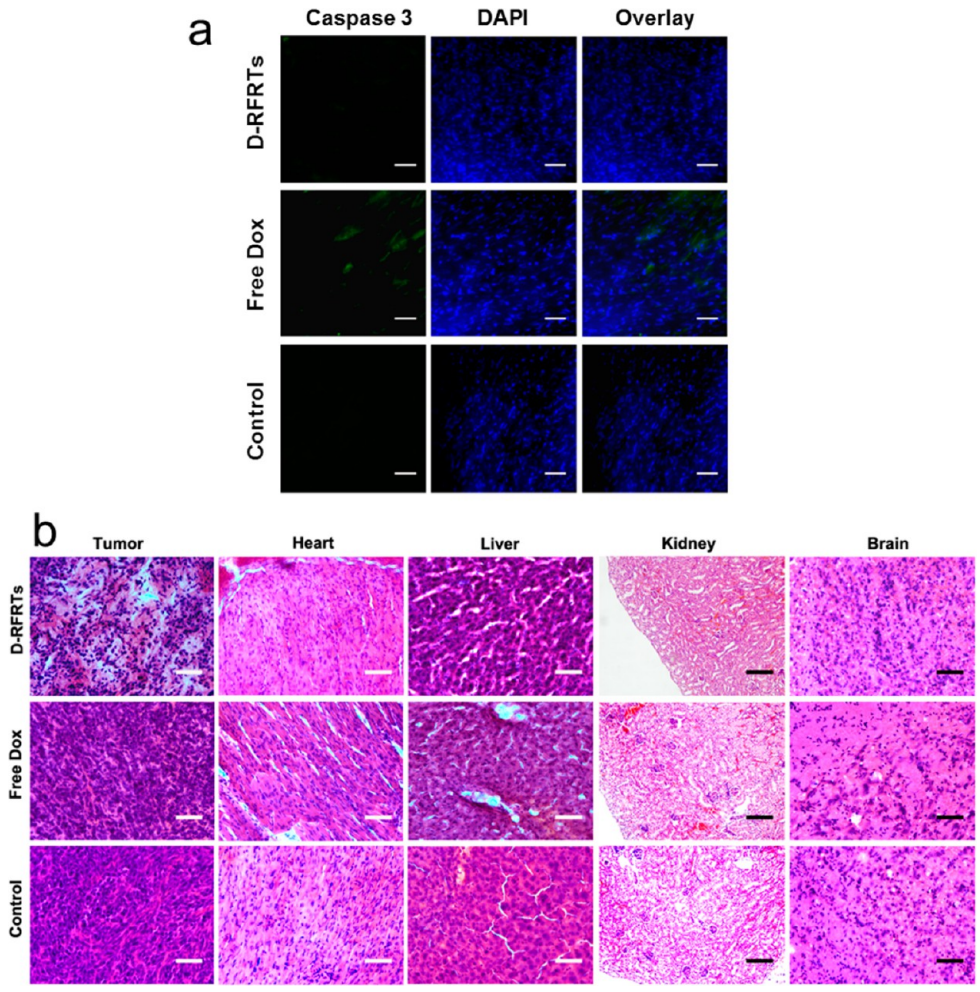

Figure 5. (a) Immunofluorescence staining of caspase-3 for myocardium from D-RFRTs, free Dox and PBS treated mice. Blue, DAPI; green, caspase-3. Scale bar: 50 μm. (b) H&E staining results from tumors and major organs. More necrosis was found in the tumors from the D-RFRT group than that from the Dox group. No obvious pathological abnormality was found in other normal tissues for D-RFRT treated mice. Scale bar, 50 μm.

that facilitates the internalization of the drug through the threefold channel, which is otherwise not accessible by Dox.

We observed significantly improved pharmacokinetics of Dox by using RFRTs as a drug carrier. These include an extended circulation half-life, reduced cardiotoxicity, and much higher tumor uptake. Immunostaining results confirmed the role of RGD−integrin interaction in the tumor selectivity. In addition to this specific interaction, we believe that the EPR effect has also played a role. It is noted that the gel-filtration chromatography study found a small portion (less than 4%) of particle clustering in D-RFRTs. The stability, cellular uptake, *in vivo* imaging, and therapy study results, however, found no significant impact of the clustering on tumor targeting and drug delivery.

The surface engineering and drug loading techniques developed in the current study can be extended to construct other FRT-based nanoplatforms. For instance, different targeting motifs (α-melanocyte stimulating hormone, bombesin, folic acid, just to name a few), or combinations of motifs, can be introduced onto FRTs to allow delivery to a different target.[28] It was reported recently that many cancer cell lines express transferrin receptor 1 (TfR1) to which FRTs can be bound,[29] suggesting the possibility of using parent FRTs as a drug carrier. It is worth noting that the relatively low carrier extravasation rate observed in the current study is due to the association of RFRTs with integrin $\alpha_v\beta_3$ expressed on tumor endothelial cells. For a ligand whose target is on tumor cells instead of tumor vasculature, we expect to see a much higher extravasation rate. In addition to Dox, it is expected that other metal-drug complexes can be loaded *via* a similar route.

In summary, we showed that Dox can be efficiently encapsulated into RFRT nanocages by using Cu(II) as a helper agent. The drug-loaded RFRTs kept integrin selectivity, which was confirmed by both *in vitro* and *in vivo* imaging. Therapeutic studies on a subcutaneous U87MG tumor model found improved tumor

suppression and reduced cardiotoxicity. Overall, FRT-based drug delivery is a safe and efficient technology and holds great potential in clinical translation.

METHODS

Expression and Purification of RFRTs and FRTs. The protocol is similar to the one reported previously.[2] In brief, PCR was used to amplify FRTs/RFRTs from cDNA using respective primers to introduce NcoI and XhoI restriction sites flanking the normal start and stop codons. The double digested PCR product was ligated into NcoI/XhoI digested plasmid pRSF with T4 DNA ligase and the ligation mixture was used to transform competent cells of *Escherichia coli* XL1-Blue by standard procedures. The resulting pRSF/FRT (or RFRT) plasmids were screened by appropriate restriction digests, verified by DNA sequencing, and then used to transform the expression strain *E. coli* BL21(DE3). For expression, a 1 L LB-kanamycin (50 μg/mL) culture of *E. coli* BL21(DE3)/RFRT was grown at 37 °C until an OD600 of 0.8 was reached. For induction, 1 mM IPTG was added to the culture and the culture was heated at 37 °C for 4 h. After sonication, the cell lysate was centrifuged at 10 400 rpm (12 930*g*) for 30 min to remove cell debris. The supernatant was heated at 60 °C for 10 min and centrifuged at 13 000 rpm for 30 min to remove the precipitates. 2-Mercaptoethanol (10 mM) was added to stabilize the product. The raw product was purified by HPLC using a Superose 6 size exclusion column. The concentration of FRTs/RFRTs was determined by Bradford protein assay. The purified FRTs/RFRTs were stored at −80 °C. Gel-filtration study was also performed on a Superose 6 column using PBS as the mobile phase.

Dox Loading. For Dox loading, Dox (1 mg/mL) was first incubated with Cu(II) (1 mM) at room temperature for 20 min. The mixture was added into a RFRT solution (250 μg/mL) and incubated at room temperature for 120 min. The products were run through a NAP-50 column to remove free Dox and Cu(II). The loaded Dox was quantified at pH 2.0 using a fluorescence spectrometer (F-7000, Hitachi) by comparing to a standard curve. The Dox loading rate in weight percent (Dox/ferritin weight percent), was computed. The detailed of the drug loading using other helper metals are described in the Supporting Information.

Labeling RFRTs/D-RFRTs with ZW800. For labeling, 5 μL ZW800-NHS was added into 1 mL of D-RFRTs solution at 100:1 molar ratio. The mixture was incubated at 4 °C for 30 min and purified by a NAP-50 column. ZW800 was quantified by a UV−vis spectrometer by comparing to a standard curve.

Drug Release. Dox release from D-RFRTs was studied with a slide-A-lyzer dialysis device (10K MWCO, Pierce). In detail, 0.5 mL of D-RFRTs was loaded onto the device and the device was immersed in 15 mL of PBS (pH 7.4 and pH 5.0). At selective time points, 0.5 mL of releasing medium was taken from the tube and replaced with 0.5 mL of fresh medium. The Dox concentrations in the sample solutions were measured by fluorescence spectrometry by comparing to a standard curve. Experiments were performed in triplicate. Drug release in FBS and a DTT solution was studied similarly.

Cellular Uptake and Viability Assays. U87MG human glioblastoma cells were cultured in MEM supplemented with 2 mmol/L L-glutamine, 1.5 g/L sodium bicarbonate, 0.1 mmol/L nonessential amino acids, 1.0 mmol/L sodium pyruvate, and 10% fetal bovine serum at 37 °C in a humidified atmosphere with 5% CO_2. For cellular uptake, 10^5 U87MG cells were seeded onto each well of a 4-chamber slide (Lab-Tek) one day prior to the studies. For cellular imaging, D-RFRTs were added into the chambers to reach a final concentration of 20 μg RFRT/mL. In the control groups, free c(RGDyK) at a 20× molar concentration was added 1 h prior to the addition of ZW800 labeled D-RFRTs. At selective time points, the incubation was stopped and the cells were rinsed 5 times with PBS (pH 7.4) and fixed with 75% ethanol at 4 °C. The slides were mounted with DAPI containing mounting medium (Vector, Inc.) and imaged under an Olympus X71 fluorescence microscope. The cell viability was assessed by MTT assays using a gradient of D-RFRTs (Dox concentrations of 1, 5, 10, 25, 50, and 100 μg/mL). For controls, free Dox and Cu(II)-bearing RFRTs were studied.

Animal Models. Animal studies were performed according to a protocol approved by the Institutional Animal Care and Use Committee (IACUC) of University of Georgia. The U87MG tumor models were generated by subcutaneously injecting 5×10^6 cells in 100 μL of PBS into the right shoulders of 4−6 week old athymic nude mice (Harlan).

Circulation Half-Lives. To determine the circulation half-lives, D-RFRTs and Dox (5 mg Dox/kg) were iv injected into healthy nude mice. At selected time points, 2−10 μL of blood was collected from the tail vein and dissolved in heparin solution (1000 U/mL in PBS). The Dox was extracted by acidified 2-propanol, and the content was detected on a microplate reader by comparing to a standard curve. The results were plotted as the Dox level against time. The circulation half-lives were evaluated by fitting the results into a two-phase decay model.

***In Vivo* Imaging Studies.** The imaging studies started when tumors reached a size between 200 and 500 mm^3. D-RFRTs and Dox at the same Dox dose (10 mg/kg) were injected into U87MG bearing mice ($n = 3$). Images were taken on a Maestro II imaging system (PerkinElmer) at 1, 4, and 24 h post injection (p.i.) time points. After the 24 h scan, all the mice were sacrificed. Tumors as well as major organs were harvested, weighed, and subjected for *ex vivo* imaging. The images were unmixed by the vendor provided software. ROIs were circled around the organs, and the optical intensities (in total scaled counts/s) were read by the Maestro software. After the imaging, the tumors were snap-frozen in O.C.T. (Tissue-Tek) and stocked in a −80 °C freezer. The tumors were sectioned into 10 μm slices and subjected to integrin β_3 staining.

Therapy Studies. For therapy studies, 20 U87MG tumor bearing mice were randomly divided into 4 groups and iv injected with D-RFRTs (5 mg Dox/kg), free Dox (5 mg Dox/kg), RFRTs and PBS every three days for 2 weeks ($n = 5$, initial average tumor size was 29.45 mm^3). The tumor size and body weight were inspected every three days. The tumor size was calculated with the formula: tumor volume = length × $(\text{width})^2/2$. Measured values were presented as mean ± SD. The one-tailed Student's *t* test was used for comparison among groups, with *P*-values of 0.05 or less representing statistical significance. After therapy, major organs as well as tumors were collected and snap-frozen in O.C.T. at −80 °C. These tissues were sectioned into 10 μm slices for Caspase 3 and H&E staining. The anti-caspase 3 antibody (Abcam) detects only the cleaved p17 fragment, but not the precursor form.

Conflict of Interest: The authors declare no competing financial interest.

Acknowledgment. This work was supported by an NCI/NIH R00 grant (5R00CA153772), a UGA startup grant, and the Intramural Research Program of NIBIB, NIH. T. Todd was supported by a Philbrook scholarship. We thank Prof. J. Frangioni at Harvard Medical School for generously providing the ZW800 dye. We thank Dr. C. Guo and Prof. B. Xu at UGA for helping with the AFM analysis.

Supporting Information Available: SDS-PAGE analyses, dynamic light scattering studies, cellular uptake study of D-RFRTs, and body weight change for U87MG bearing mice treated with D-RFRTs, free Dox, RFRTs, and PBS. This material is available free of charge *via* the Internet at http://pubs.acs.org.

REFERENCES AND NOTES

1. Maham, A.; Tang, Z.; Wu, H.; Wang, J.; Lin, Y. Protein-Based Nanomedicine Platforms for Drug Delivery. *Small* **2009**, *5*, 1706–1721.

2. Lin, X.; Xie, J.; Niu, G.; Zhang, F.; Gao, H.; Yang, M.; Quan, Q.; Aronova, M. A.; Zhang, G.; Lee, S.; *et al.* Chimeric Ferritin Nanocages for Multiple Function Loading and Multimodal Imaging. *Nano Lett.* **2011**, *11*, 814–819.
3. Sun, C.; Yang, H.; Yuan, Y.; Tian, X.; Wang, L.; Guo, Y.; Xu, L.; Lei, J.; Gao, N.; Anderson, G. J.; *et al.* Controlling Assembly of Paired Gold Clusters within Apoferritin Nanoreactor for *in Vivo* Kidney Targeting and Biomedical Imaging. *J. Am. Chem. Soc.* **2011**, *133*, 8617–8624.
4. Douglas, T.; Stark, V. T. Nanophase Cobalt Oxyhydroxide Mineral Synthesized within the Protein Cage of Ferritin. *Inorg. Chem.* **2000**, *39*, 1828–1830.
5. Wong, K. K. W.; Mann, S. Biomimetic Synthesis of Cadmium Sulfide-Ferritin Nanocomposites. *Adv. Mater.* **1996**, *8*, 928–932.
6. Geninatti Crich, S.; Bussolati, B.; Tei, L.; Grange, C.; Esposito, G.; Lanzardo, S.; Camussi, G.; Aime, S. Magnetic Resonance Visualization of Tumor Angiogenesis by Targeting Neural Cell Adhesion Molecules with the Highly Sensitive Gadolinium-Loaded Apoferritin Probe. *Cancer. Res.* **2006**, *66*, 9196–9201.
7. Yang, Z.; Wang, X.; Diao, H.; Zhang, J.; Li, H.; Sun, H.; Guo, Z. Encapsulation of Platinum Anticancer Drugs by Apoferritin. *Chem. Commun.* **2007**, 3453–3455.
8. Dominguez-Vera, J. M. Iron(Iii) Complexation of Desferrioxamine B Encapsulated in Apoferritin. *J. Inorg. Biochem.* **2004**, *98*, 469–472.
9. Lin, X.; Xie, J.; Zhu, L.; Lee, S.; Niu, G.; Ma, Y.; Kim, K.; Chen, X. Hybrid Ferritin Nanoparticles as Activatable Probes for Tumor Imaging. *Angew. Chem., Int. Ed.* **2011**, *50*, 1569–1572.
10. Uchida, M.; Flenniken, M. L.; Allen, M.; Willits, D. A.; Crowley, B. E.; Brumfield, S.; Willis, A. F.; Jackiw, L.; Jutila, M.; Young, M. J.; *et al.* Targeting of Cancer Cells with Ferrimagnetic Ferritin Cage Nanoparticles. *J. Am. Chem. Soc.* **2006**, *128*, 16626–16633.
11. Cai, W.; Chen, X. Multimodality Molecular Imaging of Tumor Angiogenesis. *J. Nucl. Med.* **2008**, *49*), 113S–128S.
12. Millard, M.; Odde, S.; Neamati, N. Integrin Targeted Therapeutics. *Theranostics* **2011**, *1*, 154–188.
13. Ye, Y.; Chen, X. Integrin Targeting for Tumor Optical Imaging. *Theranostics* **2011**, *1*, 102–126.
14. Chen, K.; Chen, X. Integrin Targeted Delivery of Chemotherapeutics. *Theranostics* **2011**, *1*, 189–200.
15. Feng, M.; Yang, Y.; He, P.; Fang, Y. Spectroscopic Studies of Copper(Ii) and Iron(Ii) Complexes of Adriamycin. *Spectrochim. Acta, Part A* **2000**, *56*, 581–587.
16. May, P. M.; Williams, G. K.; Williams, D. R. Speciation Studies of Adriamycin, Quelamycin and Their Metal-Complexes. *Inorg. Chim. Acta* **1980**, *46*, 221–228.
17. Shokeen, M.; Anderson, C. J. Molecular Imaging of Cancer with Copper-64 Radiopharmaceuticals and Positron Emission Tomography (Pet). *Acc. Chem. Res.* **2009**, *42*, 832–841.
18. Cai, W.; Shin, D. W.; Chen, K.; Gheysens, O.; Cao, Q.; Wang, S. X.; Gambhir, S. S.; Chen, X. Peptide-Labeled near-Infrared Quantum Dots for Imaging Tumor Vasculature in Living Subjects. *Nano Lett.* **2006**, *6*, 669–676.
19. Chen, K.; Xie, J.; Xu, H.; Behera, D.; Michalski, M. H.; Biswal, S.; Wang, A.; Chen, X. Triblock Copolymer Coated Iron Oxide Nanoparticle Conjugate for Tumor Integrin Targeting. *Biomaterials* **2009**, *30*, 6912–6919.
20. Li, Z. B.; Wu, Z.; Chen, K.; Chin, F. T.; Chen, X. Click Chemistry for ^{18}F-Labeling of RGD Peptides and microPET Imaging of Tumor Integrin $\alpha_v\beta_3$ Expression. *Bioconjugate Chem.* **2007**, *18*, 1987–1994.
21. Choi, H. S.; Nasr, K.; Alyabyev, S.; Feith, D.; Lee, J. H.; Kim, S. H.; Ashitate, Y.; Hyun, H.; Patonay, G.; Strekowski, L.; *et al.* Synthesis and *in Vivo* Fate of Zwitterionic near-Infrared Fluorophores. *Angew. Chem., Int. Ed.* **2011**, *50*, 6258–6263.
22. Quan, Q.; Xie, J.; Gao, H.; Yang, M.; Zhang, F.; Liu, G.; Lin, X.; Wang, A.; Eden, H. S.; Lee, S.; *et al.* HSA Coated Iron Oxide Nanoparticles as Drug Delivery Vehicles for Cancer Therapy. *Mol. Pharmaceutics* **2011**, *8*, 1669–1676.
23. Brewer, G. J. Copper Toxicity in the General Population. *Clin. Neurophysiol.* **2010**, *121*, 459–460.
24. Lefrak, E. A.; Pitha, J.; Rosenheim, S.; Gottlieb, J. A. A Clinicopathologic Analysis of Adriamycin Cardiotoxicity. *Cancer* **1973**, *32*, 302–314.
25. Kheirolomoom, A.; Mahakian, L. M.; Lai, C. Y.; Lindfors, H. A.; Seo, J. W.; Paoli, E. E.; Watson, K. D.; Haynam, E. M.; Ingham, E. S.; Xing, L.; *et al.* Copper-Doxorubicin as a Nanoparticle Cargo Retains Efficacy with Minimal Toxicity. *Mol. Pharmaceutics* **2010**, *7*, 1948–1958.
26. Abraham, S. A.; McKenzie, C.; Masin, D.; Ng, R.; Harasym, T. O.; Mayer, L. D.; Bally, M. B. *In Vitro* and *in Vivo* Characterization of Doxorubicin and Vincristine Coencapsulated within Liposomes through Use of Transition Metal Ion Complexation and pH Gradient Loading. *Clin. Cancer Res.* **2004**, *10*, 728–738.
27. Takahashi, T.; Kuyucak, S. Functional Properties of Threefold and Fourfold Channels in Ferritin Deduced from Electrostatic Calculations. *Biophys. J.* **2003**, *84*, 2256–2263.
28. Lee, S.; Xie, J.; Chen, X. Peptides and Peptide Hormones for Molecular Imaging and Disease Diagnosis. *Chem. Rev.* **2010**, *110*, 3087–3111.
29. Fan, K.; Cao, C.; Pan, Y.; Lu, D.; Yang, D.; Feng, J.; Song, L.; Liang, M.; Yan, X. Magnetoferritin Nanoparticles for Targeting and Visualizing Tumour Tissues. *Nat. Nanotechnol.* **2012**, *7*, 459–464.